SCOUR PROTECTION CALCULATIONS FOR AN OFFSHORE ENERGY ISLAND USING DETAILED WAVE AND CFD FLOW MODELING

Floris de Wit[1], Eelco Bijl[2], Sam Bom[1], Yannick Steenman[1], Leen Baelus[3], Koen Van Doorslaer[4], Pierre-Yves Guillermin[5]

This paper presents a new and promising method for calculating the rock diameter required for scour protection systems. The methodology consists of performing detailed SWASH wave simulations and TUDflow3D flow simulations to accurately assess the combined bed-shear stress and movement for scour protection stones. The results of the numerical model are compared with measurements from 3D laboratory experiments. As a case study, the methodology is applied to the Princess Elisabeth Island project in the North Sea, 45 km off the Belgian coast. This methodology is well able to predict the areas that are most prone to rock movement under extreme conditions.

Keywords: Scour protection; Princess Elisabeth Island; Energy island; Waves; Currents; SWASH; TUDFlow

INTRODUCTION

The transition to renewable energy is one of the defining challenges of the 21st century, with offshore wind power playing a central role in achieving global climate targets (Rodrigues et al., 2015). As countries strive to meet emission reduction goals, large-scale offshore wind farms are being developed at an unprecedented pace. These projects are transforming coastal and marine environments into key hubs of clean energy production, marking a shift away from fossil fuel reliance.

One of the critical challenges of this transition lies in efficiently transmitting the energy generated offshore to the mainland (Ackermann, 2005). Offshore wind turbines produce electricity that must be transported via subsea cables to onshore grids. Traditionally, this involves converting the power at nearby offshore platforms before transmitting it onshore. However, the rapid expansion of offshore wind farms has led to increasingly complex cable networks, requiring multiple platforms to handle the growing demand. Although functional, this approach introduces significant logistical, spatial, and economic constraints.

To address these challenges, the concept of an offshore energy island has emerged as a innovative solution. Energy islands centralize the collection and conversion of power from offshore wind farms, providing a scalable and economically viable alternative to multiple platforms (Jansen et al., 2022). This approach also allows for the integration of renewable energy sources with regional and international electricity grids.

In 2024, the construction of the world's first energy island commenced, the Princess Elisabeth Island, in the Belgian coastal zone. This landmark project from ELIA, the Transmission System Operator in Belgium, with a planned capacity of up to 3.5 GW, will connect offshore wind farms to the mainland and create vital interconnections with the electricity grids of neighboring countries. As a pioneering effort, it represents a significant step towards achieving a robust and interconnected European energy market while addressing the growing demands of offshore renewable energy production.

One of the technical challenges of constructing an energy island is that it is a large structure located in the open sea, where it is fully exposed to waves and currents. These can create strong hydrodynamic forces around the base of the island, leading to sediment erosion, commonly known as scour (Whitehouse et al., 2011). If left unprotected, the scour can progressively undermine the island's foundation, compromising its structural stability and potentially leading to severe damage or failure of the infrastructure.

To ensure the stability and safety of the island, the implementation of effective scour protection is essential. This typically involves placing layers of rock or other protective materials around the base of the island to counteract sediment displacement caused by hydrodynamic forces. The design of scour protection systems requires careful consideration of site-specific conditions, including wave heights, current velocities, and seabed composition.

Commonly, the diameter of the scour protection stones is calculated using formulae that account for the combined effects of waves and currents (De Vos et al., 2012). For this specific project, this poses two problems. Firstly, in contrast to commonly applied offshore structures (e.g., monopiles or tripods),

[1]Svašek Hydraulics, Rotterdam, The Netherlands
[2]CDR International, Amersfoort, The Netherlands
[3]IMDC, Antwerp, Belgium
[4]DEME nv, Zwijndrecht, Belgium
[5]ELIA, Brussels, Belgium

it is unknown how the undisturbed wave and flow conditions are affected by the presence of the island. Secondly, the presence of the island results in spatially complex wave patterns. For perpendicular waves standing wave patterns will occur, for which it is difficult to predict the near-bed orbital velocities based on simple equations (e.g., Soulsby (2006)) because the highest orbital velocities occur where the standing wave height is lowest. For oblique waves, mach stem wave reflection (might) occur (Tanaka, 1993), in which the waves propagate along the island walls. Both processes are not captured by models and theories based on linear wave theory.

In this study, the diameter of the rock protection will be calculated with a formula for large rock under combined current and wave load. In contrast to common practice, in which the formula depends on undisturbed flow and wave velocities, including safety factors, we will apply detailed numerical flow and wave modeling to predict spatially varying flow and wave velocities. Subsequently, the results of the modeling-based scour protection design will be compared with measurements from 3D laboratory experiments.

PRINCESS ELISABETH ISLAND

Background, location and design

The Princess Elisabeth Island is an innovative artificial energy island under construction approximately 45 kilometers off the Belgian coast in the North Sea, in an approximate depth of 20 m (see Figure 1). Named after Belgium's Crown Princess Elisabeth, this pioneering project is the world's first of its kind, designed to function as a central electricity hub. Its primary role is to consolidate cables from offshore wind farms located in Belgium's second offshore wind zone, known as the Princess Elisabeth Zone, thereby facilitating the transmission of renewable energy to the mainland.

TM Edison, a joint venture from the Belgian marine contractors DEME and Jan De Nul, has started the construction. The island perimeter will consist of 23 concrete caissons, resulting in approximate island dimensions of 520 x 230 m (van Doorslaer et al., 2024). The interior of the island will be filled with sand and, on the relatively sheltered east side, a small harbor will be constructed allowing for CTV vessels. The island includes 95 cable landings which are capable to receive subsea power cables, consisting of HVAC inter-array cables, export cables, and HVDC cables (Bijl et al., 2024). The island orientation is such that it is aligned with the predominant tidal flow direction, which is towards the north-northeast for flood flow and south-southwest for ebb flow.

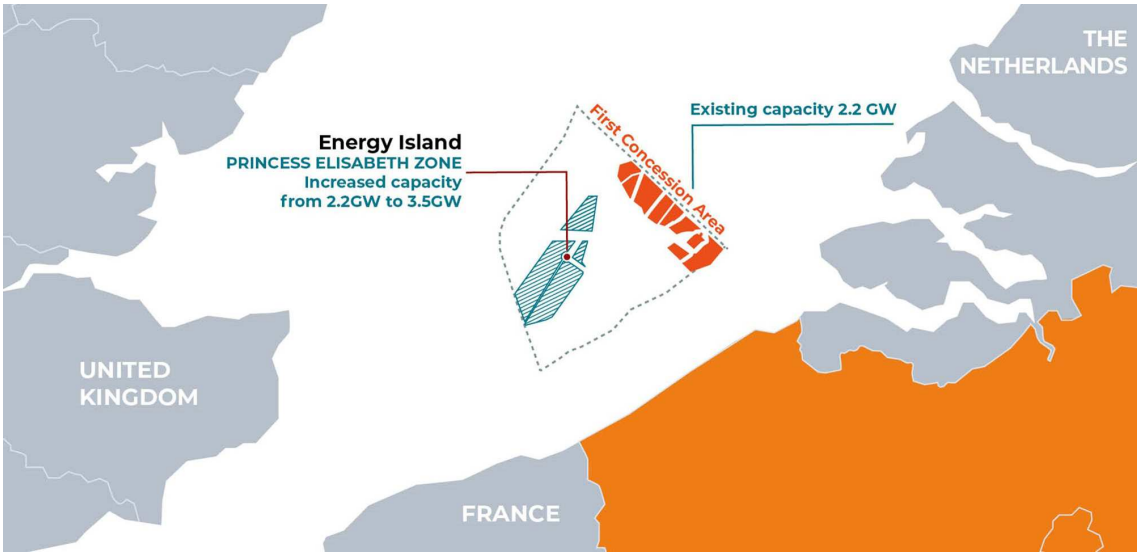

Figure 1: Schematic map showing the Belgian windfarm zones and the Princess Elisabeth Island location in the southern North Sea [source: www.elia.be].

Metocean conditions

Metocean conditions have been obtained from a dedicated metocean study, performed specifically for this project (Svasek Hydraulics, 2022). Based on 40 years of hydrodynamic and wave modeling using calibrated and validated models, long-term timeseries have been obtained. These timeseries formed the basis for an extreme value analysis. In this study, as an example, we focus on the joint probability of flow velocities with a return period of 10 years combined with waves with a return period of 100 years during low water levels. Low water levels are chosen, as this is commonly governing for the scour protection stability.

The 10-year return period flow velocities for flood and ebb conditions are shown in Table 1. The highest velocities occur for perfect alignment of the flow with the island orientation. However, for some locations surrounding the island, this might not be the governing condition as these locations might be in the lee of the island or in areas of flow separation. Therefore, it is important to consider a broader range of flow directions. As a consequence, additional velocity magnitudes have been derived that are valid for slight angles of inclination.

Table 1: Metocean flow conditions with RP = 10 years

Direction w.r.t. island centreline (°)	-20	-10	0	10	20
Flood flow to NNE magnitude (m/s)	1.00	1.30	1.54	1.46	1.27
Ebb flow to SSW magnitude (m/s)	0.90	1.24	1.48	1.23	0.88

In contrast to the tidal currents, waves approach the island from a wider variety of directions. As can be seen in Table 2, the highest waves originate from the north, northwest, and west-southwest. Because the southeast side is relatively sheltered against these directions, waves from the southern directions are also included. Waves that reflect against a vertical caisson wall will result in standing wave patterns, with distinct areas of increased and decreased wave heights and associated orbital velocities. These patterns are predominantly determined by the wave period and wave direction. Furthermore, for certain angles of obliqueness, mach stem reflection occurs in which the waves propagate parallel to the island walls, potentially resulting in further steepening and breaking. Therefore, for each storm direction, a combination of three directions and three wave periods is considered. Water levels are based on the joint probability of waves, tide and surge. North and northwestern storms commonly coincide with positive surge levels, whereas southwestern storms can also coincide with negative surge. This explains the distinction in water levels in Table 2.

Table 2: Metocean wave and water level conditions with RP = 100 years

Storm direction	Wave height (m)	Peak period (s)	Peak direction (degN)	Water level (m)
North	7.0	10.3, 11.3, 12.3	350, 0, 10	+2.3 m+LAT
Northwest	5.5	8.4, 8.9, 9.4	297.5, 307.5, 317.5	+2.3 m+LAT
Westsouthwest	5.7	7.5, 8.2, 8.9	237.5, 247.5, 257.5	+0.7 m+LAT
South	3.7	6.5, 6.8, 7.1	170, 180, 190	+0.7 m+LAT

METHODOLOGY

Scour protection formula

To predict the stone diameter of the scour protection, we apply the formula of Van Rijn (2019), which is valid for large rocks under combined load by waves and currents:

$$D_{50} = \frac{\gamma_s \left[0.013 \left(\frac{h}{\alpha}\right)^{-0.3} (\gamma_{str} U_c)^2 + 0.045 \left(\frac{T_p}{\alpha}\right)^{-0.3} (\gamma_{str} U_w)^{1.7} \right]^{1.4}}{\left[\frac{\rho_s - \rho_w}{\rho_w} g K_\alpha r \theta_{cr,shields} \right]^{1.4}} \quad (1)$$

Input parameters for this formula are presented in Table 3. An important parameter is the movement reduction factor r. Basically, this quantifies the amount of movement and is defined as:

- r = 0.4: occasional particle movement at some locations (≈0.1% of surface is moving);

- r = 0.6: frequent particle movement at some locations (≈1% of surface is moving);
- r = 0.8: frequent particle movement at many locations (≈10% of surface is moving);
- r = 1.0: frequent particle movement at nearly all locations (≈50% of surface is moving).

K_α is a factor accounting for the reduced stability for stones located under bed slope α, which is in this study calculated by the following simplified expression:

$$K_\alpha = cos(\alpha) \tag{2}$$

This is an adaptation from the longitudinal and lateral bed slope factors suggested by Van Rijn (2019). This is chosen because the original expressions do not seem applicable for the falling apron part of the scour protection. For a falling apron, stones are encapsulated in the seabed and interlocked by the stones above and below. This significantly increases the stability, which is not accounted for by the original expressions. A sensitivity analysis of this choice is presented in the Appendix of this paper.

Table 3: Parameters in the scour protection formula

Parameter	Description	Value
D_{50}	Rock size diameter (m)	to be calculated
g	Gravitational acceleration (m/s^2)	9.81
h	Total water depth (m)	Figure 2
K_α	Bed slope factor (-)	Eq. 2
r	Movement reduction factor (-)	0.4-1.0
T_p	Peak wave period (s)	Table 2
U_c	Depth-averaged current velocity (m/s)	TUDflow3D model
U_w	Near-bed wave orbital velocity (m/s)	SWASH model
α	Bed roughness coefficient (-)	2.5
γ_s	Safety factor (-)	1.2
γ_{str}	Structure-enhanced turbulence factor (-)	1.0-1.5
$\theta_{cr,shields}$	Critical Shields number (-)	0.055
ρ_s	Rock density (kg/m^3)	2650
ρ_w	Water density (kg/m^3)	1025

Equation (1) can give a good first estimate of the required diameter of the stones. However, in practice, the full range of stone diameters is not available nor is it possible to distribute them spatially according to complex spatial maps that might arise from Equation (1). From a constructability perspective, the heaviest part of the scour protection consists of one or a few stone classes. Therefore, Equation (1) is re-written such that it quantifies the amount of movement r for the D_{50} of a specific stone size class:

$$r = \frac{0.013\left(\frac{h}{\alpha}\right)^{-0.3}(\gamma_{str}U_c)^2 + 0.045\left(\frac{T_p}{\alpha}\right)^{-0.3}(\gamma_{str}U_w)^{1.7}}{\frac{\rho_s-\rho_w}{\rho_w}gK_{\alpha1}K_{\alpha2}\theta_{cr,shields}}\left(\frac{\gamma_s}{D_{50}}\right)^{1/1.4} \tag{3}$$

In this study, we consider the stability of a scour protection for two different stone size classes: 60-300 kg and 3000-1000 kg. The representative D_{50} for these classes is 0.45 and 0.725 m, respectively.

Flow modeling

When the undisturbed metocean flow encounters the energy island, the obstruction of the flow will result in flow accelerations, as well as horizontal and vertical turbulent eddies that affect the velocity field. To predict spatial variations in flow velocities $U_c(x, y)$, we apply the fully three-dimensional CFD model TUDflow3d, which solves turbulent flow around the island for design flood and ebb conditions (de Wit, 2015). The model domain is discretized using 48 vertical layers and has a horizontal grid spacing of 2 x 2 m. The bathymetry in close proximity to the island is shown in Figure 2. A large-eddy-simulation turbulence model was employed to accurately capture the most influential eddies. Given that Equation (1) requires stationary flow velocities values, the resolved flow fields are time-averaged over the simulation

duration of six hours. This duration is based on a sensitivity analysis and corresponds to approximately 20 times the timescale of the dominant horizontal eddies. It is noted that in reality the peak tidal flow conditions do not reside for six hours. However, simulating for shorter durations showed too much spatial dependence on the number of eddies that a certain location has encountered.

The strongest ebb and flood velocities are nearly perfectly aligned with the longitudinal island orientation. However, only accounting for perfectly aligned strong velocities will not be the governing conditions for all locations. For instance, flow wakes with low flow velocities will occur at the two lateral sides of the island. However, the governing flow velocities around the lateral sides of the island will occur when the flow has a slight inclination angle, instead of being aligned with the island orientation. Therefore, based on the tidal ellipse, also flow directions with an inclination angle of -20, -10, 10, and 20 degrees are considered. Doing so for both ebb and flood conditions results in a total of 10 simulations.

For each of the simulations, $U_c(x, y)$ is obtained by averaging the velocities over the simulation time and water depth. It is noted that a sensitivity check has been performed, in which the combination of maximum flow velocities with a turbulence factor of 1 were compared to time-averaged flow velocities with a turbulence factor of 1.5. The latter proved governing and is therefore applied in this study. Finally, the combined flow conditions with a return period of 10 years are determined in each spatial location by taking the maximum value of the 10 simulations.

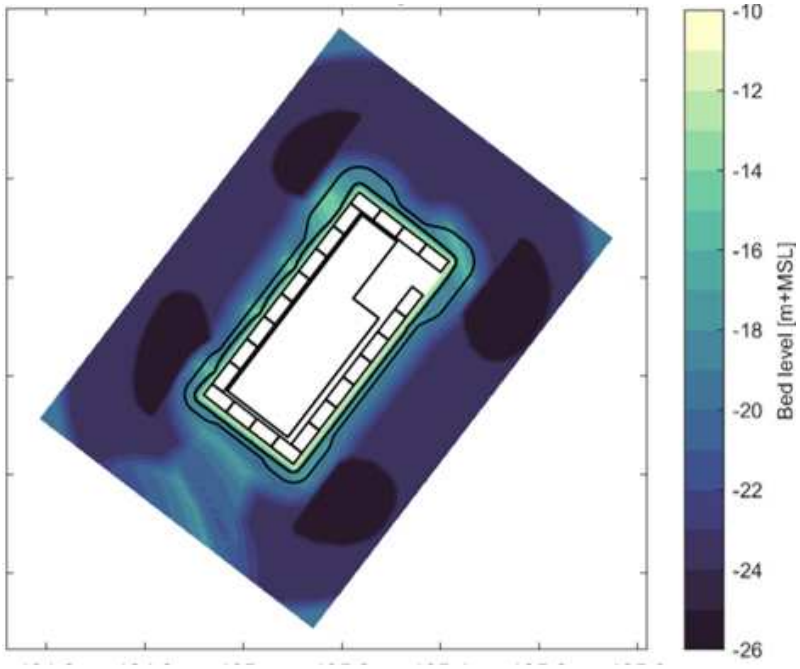

Figure 2: Bed level in the near-vicinity of the Princess Elisabeth Energy Island. Black lines indicate the 23 caissons and the extent of the proposed scour protection. At the island corners, deeper scour hole areas are included based on preliminary morphological simulations. Please note that the model domains are larger then what is shown in this Figure.

Wave modeling

Storm waves that encounter the island's caisson walls result in partially standing wave patterns, nonlinear steep waves propagating along the island walls, strong diffraction around the sharp corners, and potentially wave breaking. To resolve these phenomena, a detailed nonlinear and phase-resolving wave model is required. To this end, the SWASH wave model is used, which solves the nonlinear shallow water equations including the nonhydrostatic pressure (Zijlema et al., 2011).

The SWASH model domain has a length of 1800 x 1200 m, discretized with horizontal cells of 1 x 1 m. In the vertical, two layers are applied to properly resolve the wave dispersion. Depending on the incoming wave direction, cyclic boundary conditions are applied at the lateral boundaries to avoid boundary shadow effects. Waves are generated using the source function wave maker (Vasarmidis et al., 2021), which

is particularly good in dealing with waves reflected back towards the wavemaker. Wave and water level boundary conditions are shown in Table 2.

Typically, bed shear stress formulae (e.g. Grant and Madsen (1979); Sleath (1991); Soulsby (1995)) calculate wave orbital velocities as a function of the local wave height. However, in standing wave patterns this assumption is not valid because highest velocities are actually expected where the standing wave height is minimum (Iwagaki and Hirayama, 1975). Furthermore, these calculations as a function of the local wave height rely on wave propagation according to linear wave theory, which is far from valid under these nonlinear conditions including wave-structure interaction. Because the SWASH model is a time-resolving 3D model, velocity timeseries can directly be obtained from the model output, thereby removing inaccuracies associated with parameterizing the velocities as a function of e.g., the wave height and wave period. Following Wiberg and Sherwood (2008), the orbital velocities are calculated from SWASH model results according:

$$U_w = \sqrt{2(var(u' - \overline{u}) + var(v' - \overline{v}))} * K_{att} \tag{4}$$

in which u' and v' are the instantaneous velocity components and $\overline{u}$ and $\overline{v}$ the mean velocity components in x, and y-direction, respectively. K_{att} is a factor based on linear wave theory to attenuate the depth-averaged velocity towards the near-bed velocity, as required by Equation 1. The latter approach is chosen because accurate near-bed velocity estimates cannot be directly obtained from the model since only two vertical layers are used. In line with the current modeling, $U_w(x, y)$ is for each location determined as the maximum orbital velocity from the 36 individual wave simulations.

MODELING RESULTS

The flow simulations are combined by taking in each spatial point the maximum of the ten individual simulations to end up with a combined flow velocity field with a return period of 10 years (Fig. 3A). The maximum flow velocity magnitude is almost double the undisturbed metocean flow velocity, but it is located outside of the scour protection area. Due to flow separation, most of the scour protection area (indicated by a black line) encounters relatively low flow velocities. Largest influence of the currents on the scour protection is predicted in the vicinity of the corners where vortex shedding occurs.

The spatially varying wave orbital velocity field with a return period of 100 years is generated by taking the maximum of the 36 wave simulations (Fig. 3B). The highest orbital velocities are predicted at the north and west side, as these are exposed to stronger storms. It can also be seen that amplified orbital velocities occur along the corners of the island.

Substitution of both spatial velocity fields in Equation (1) results in the bed-shear stress (Fig. 3C) and the scour protection stone diameter (Fig 3D). For these calculations, the movement factor r is set to 1.0, indicative of frequent particle movement. It can be observed that stresses are highest in the northwest and the corners, necessitating the biggest rocks. It should be noted that the calculated stone sizes at the toe protection are not reliable because the stability of these large rocks is not only governed by wave and current-induced horizontal shear stresses.

For designers, the results presented in Figure 3D will not be practical, because it is not feasible to design and construct a scour protection with this much spatial detail and this much variation in stone diameter. Therefore, Equation (3) is applied to show the stability of two stone classes: 60-300 kg and 300-1000 kg (see Figure 4). As expected, higher movement is predicted for calculations with the 60-300 kg stone size class than for 300-1000 kg. For the rest, patterns are similar and comparable to 3, showing increased movement at the north of the northwest wall, and the east of the northeast wall. Further, high movement is predicted at the east and west corners.

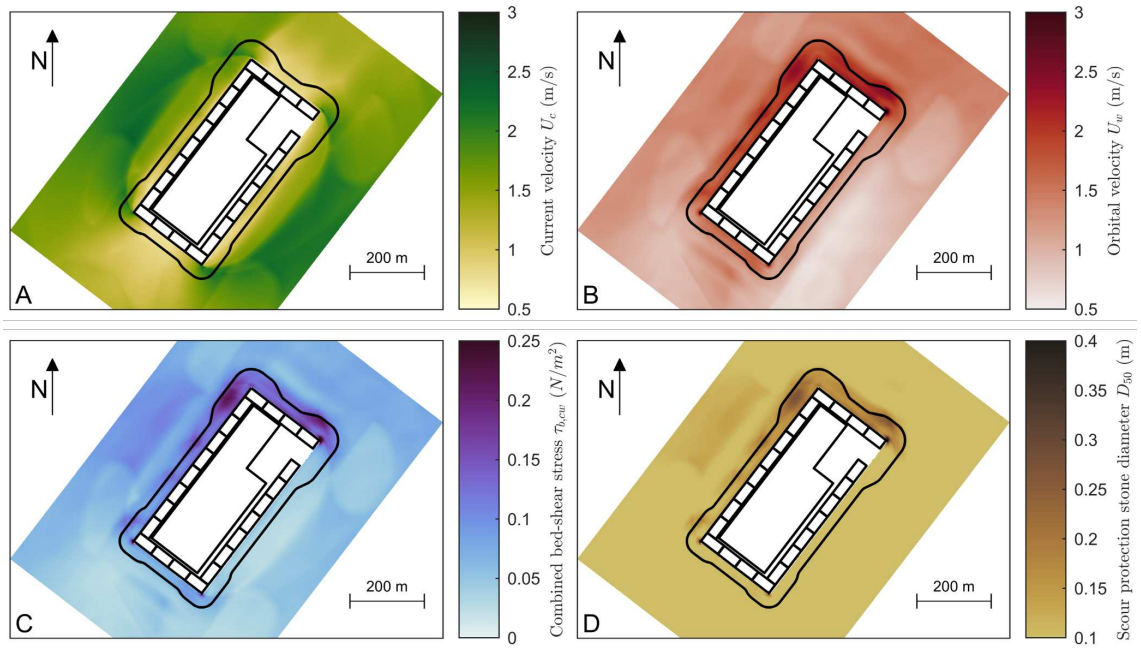

Figure 3: Spatially-varying, modeling-based scour protection design results. Panel A shows the depth-averaged currents with a return period of 10 years based on CFD modeling. Panel B shows the near-bed orbital velocity loads with a return period of 100 years, based on SWASH modeling. Panel C shows the combined bed-shear stress based on the current and wave loads. Panel D shows the corresponding required stone diameter based on Equation (1). The black lines give an indication of the proposed extent of the scour protection in Reference Design. Please note that the modeling domains were larger than these presented output domains.

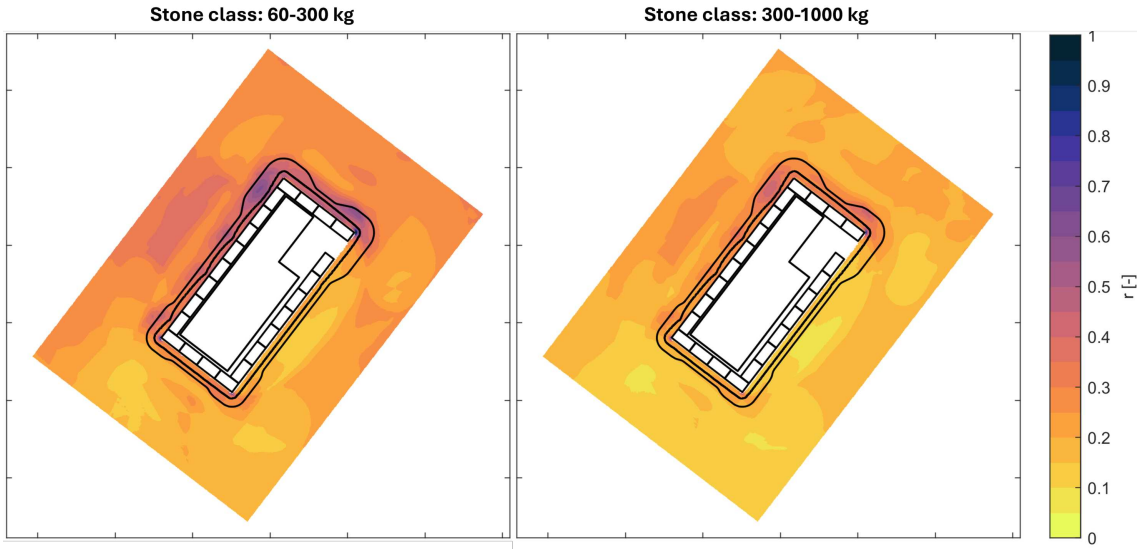

Figure 4: r-factor for stone classes 60-300 kg and 300-1000 kg.

COMPARISON WITH MEASUREMENTS

In 2023, an extensive 3D laboratory model testing campaign has been conducted at the laboratory facilities of DHI in Denmark (see Figure 5), carried out by TM Edison (Deme and Jan de Nul joint venture). The model-to-reality scale was 1:60. Froude scaling has been applied to scale the hydrodynamic conditions and stone dimensions. An overview of the test facilities without and with water is shown in Figure 5. The toe and scour protection are placed and different parts of the protection were distinguished by different color painting. In this way, after each model run, the movement could be quantified by counting the number of moving stones within a colored box and outside a colored box. The results of these tests were decisive in determining whether the detailed design satisfied the employer requirements.

In this paper, we qualitatively compare the results of the numerical model with observations from the first laboratory tests. This is done by spatially comparing the movement of stones in the laboratory simulations to numerical predictions of the movement factor. It should be noted that the comparison in this paper is not fully one-on-one. Firstly, the lab testing was for one wave direction, from the north, whereas the numerical model results are based on a combination of multiple directions. Secondly, in the lab unidirectional long-crested waves were applied, whereas in the numerical model a directionally spread wave field was used. Nevertheless, for most of the scour protection, this northern condition, including fully aligned flood flow, is assumed to be governing, making it a reasonable comparison.

Figure 5: Overview of the 3D experimental set-up, with left the basin without water with distinct colored boxes for different scour protection areas and right a snapshot of wave attack during one of the tests.

The four locations with the most substantial stone movement in the lab are visualized in Figure 6. Significant displacements occurred at the toe and scour protection of the exposed northwestern side (top left) and the lower part of the scour protection at the exposed northeastern side of the island (top right). Furthermore, significant movement of the toe protection is observed at the western and eastern corners of the island (bottom left and bottom right panels of Fig. 6, respectively). A satisfactory qualitative agreement of spatial patterns is observed when looking at the numerically predicted results (see Figure 7). Also here, highest movement is predicted at the northern part of the northwestern side and the eastern part of the northeastern side. Even though the methodology in this study is not fully applicable to the toe protection, it is satisfactory to see that the highest shear stresses in the model also occur at the western and eastern corners of the island. Interestingly, highest loads do not occur at the corner that is mostly exposed (north) but rather at the corners where the waves diffract around. It should be noted, that these were the first physical model tests. The observed movement led to an improved design by the contractor to increase the stability and meet the employer requirements. Nevertheless, these first tests proved to be a very interesting case to use for this comparative study.

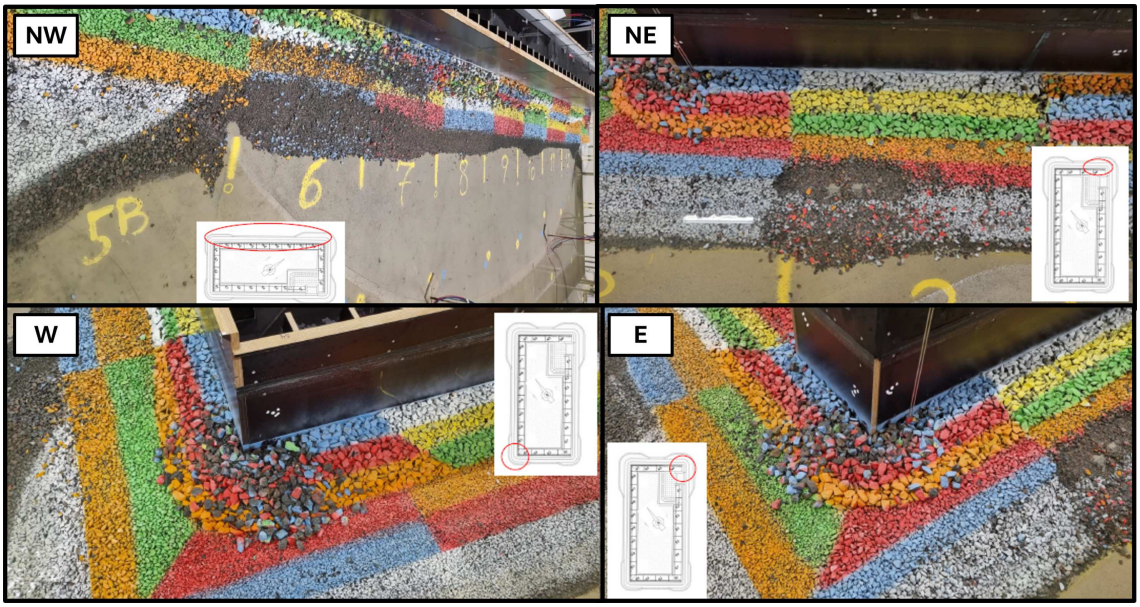

Figure 6: Pictures after the test with currents and northerly waves with a return period of 100 years. Top left shows the northwestern side, top right shows the northeastern side, bottom left shows the western corner of the island and bottom right shows the eastern corner of the island. Note that these were the first experimental tests and that the design was improved afterwards in order to meet the employer requirements.

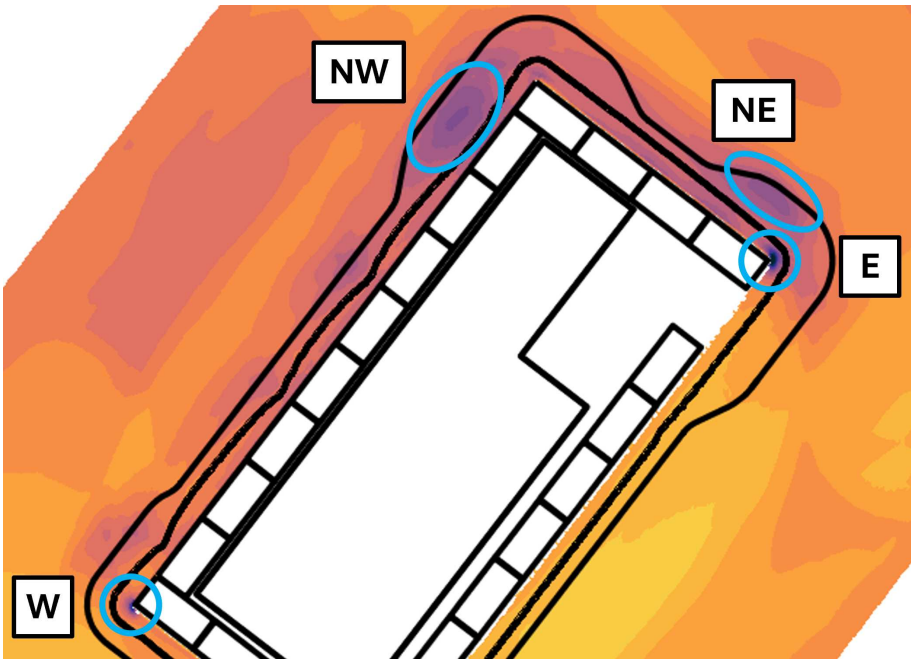

Figure 7: Zoomed in version of Figure 4A, highlighting the areas of movement with blue circles, corresponding to the movement shown in Figure 6.

CONCLUSION AND OUTLOOK

This study showed a new and promising method to calculate the required stone diameter of scour protection systems. This method consists of performing detailed SWASH wave simulations and TUDflow3D flow simulations to accurately assess the combined bed-shear stress. This is subsequently substituted in the rock stability formula of Van Rijn (2019) to provide spatial fields of the required stone size diameter for complex offshore projects. Additionally, the formula can be used inversely, such that the *r*-factor is calculated for a certain stone size class, giving the expected amount of movement for this stone class. This gives a spatial overview of the safety and robustness of the scour protection design. This can then guide further optimizations of the scour protection design, by identifying on the one hand areas where scour protection should be strengthened, and on the other hand areas where a lighter and cheaper scour protection is sufficient.

As a case study, the methodology is applied to the Princess Elisabeth Island project in the North Sea, 45 km off the Belgian coast. The combined wave and current loads have been calculated for this pioneering energy island project. A range of waves with a return period of 100 years are combined with currents with a return period of 10 years. This provided spatial overviews of the bed shear stress, the required stone size diameter and the safety factor for two stone size classes. A comparison with early 3D laboratory experiments showed that this methodology is very well able to predict the areas that are most prone to rock movement under extreme conditions. At this stage, no direct quantitative comparison is made relating the exact *r*-factor from numerical results to the amount of movement observed in the laboratory. Finally, it is proposed to perform further research for a larger range of conditions, and get a better feeling of the importance and sensitivity of all parameters in the formula of Van Rijn (2019). This will further increase the confidence and capabilities of this methodology.

ACKNOWLEDGEMENTS

We would like to acknowledge the Island Owner ELIA and all parties that have a contribution to this pioneering project. In special we would like to thank TM Edison, RoyalHaskoningDHV, and DHI for allowing us to use results from the laboratory experiments in Denmark.

References

Ackermann, T. (2005). Transmission systems for offshore wind farms. *Wind power in power systems*, pages 479–503.

Bijl, E., Baelus, L., Impens, T., van Schoten, S., and Sorensen, S. L. (2024). Stability assesment of rock bags and rock armour as protection of subsea cables landfall at an offshore energy island. In *Coastal Engineering Proceedings*.

De Vos, L., De Rouck, J., Troch, P., and Frigaard, P. (2012). Empirical design of scour protections around monopile foundations. part 2: Dynamic approach. *Coastal Engineering*, 60:286–298.

de Wit, L. (2015). *3D CFD modelling of overflow dredging plumes*. Phd thesis, Delft University of Technology, Delft, The Netherlands.

Grant, W. D. and Madsen, O. S. (1979). Combined wave and current interaction with a rough bottom. *Journal of Geophysical Research: Oceans*, 84(C4):1797–1808.

Hudson, R. Y. (1959). Laboratory investigation of rubble-mound breakwaters. *Journal of the waterways and Harbors division*, 85(3):93–121.

Iwagaki, Y. and Hirayama, H. (1975). Characteristics of the behavior of a solid particle under standing waves. *Coastal Engineering in Japan*, 18(1):63–73.

Jansen, M., Duffy, C., Green, T. C., and Staffell, I. (2022). Island in the sea: The prospects and impacts of an offshore wind power hub in the north sea. *Advances in Applied Energy*, 6:100090.

Rodrigues, S., Restrepo, C., Kontos, E., Pinto, R. T., and Bauer, P. (2015). Trends of offshore wind projects. *Renewable and sustainable energy reviews*, 49:1114–1135.

Sleath, J. F. (1991). Velocities and shear stresses in wave-current flows. *Journal of Geophysical Research: Oceans*, 96(C8):15237–15244.

Soulsby, R. (1995). Bed shear-stresses due to combined waves and currents. *Advances in coastal morphodynamics*.

Soulsby, R. (2006). Simplified calculation of wave orbital velocities.

Svasek Hydraulics (2022). Mog2 island metocean study. Technical report, Version J.

Tanaka, M. (1993). Mach reflection of a large-amplitude solitary wave. *Journal of fluid mechanics*, 248:637–661.

Van der Meer, J. W. (1987). Stability of breakwater armour layersâ€"design formulae. *Coastal engineering*, 11(3):219–239.

van Doorslaer, K., Vasarmidis, P., van Olst, B., van Koelen, L., Bijl, E., Weygers, M., Guillermin, P.-Y., Streicher, M., and Dixen, M. (2024). Physical modelling for the princess elisabeth island, overtopping design for a caisson with a double wave wall geometry. In *Coastal Engineering Proceedings*.

Van Rijn, L. (2019). Critical movement of large rocks in currents and waves. *International Journal of Sediment Research*, 34(4):387–398.

Van Rijn, L. C. (1993). *Principles of sediment transport in rivers, estuaries and coastal seas*.

Vasarmidis, P., Stratigaki, V., Suzuki, T., Zijlema, M., and Troch, P. (2021). On the accuracy of internal wave generation method in a non-hydrostatic wave model to generate and absorb dispersive and directional waves. *Ocean Engineering*, 219:108303.

Whitehouse, R. J., Harris, J. M., Sutherland, J., and Rees, J. (2011). The nature of scour development and scour protection at offshore windfarm foundations. *Marine Pollution Bulletin*, 62(1):73–88.

Wiberg, P. L. and Sherwood, C. R. (2008). Calculating wave-generated bottom orbital velocities from surface-wave parameters. *Computers & Geosciences*, 34(10):1243–1262.

Zijlema, M., Stelling, G., and Smit, P. (2011). Swash: An operational public domain code for simulating wave fields and rapidly varied flows in coastal waters. *Coastal Engineering*, 58(10):992–1012.

APPENDIX: DISCUSSION ON SLOPE EFFECTS

In this paper, the bed slope factor, K_α, is included with Equation 2. In contrast, Van Rijn (2019) suggested to apply the following two factors, for the longitudinal and lateral bed slopes, respectively:

$$K_{\alpha 1} = \frac{sin(\phi - \alpha_1)}{sin(\phi)} \tag{5}$$

$$K_{\alpha 2} = cos(\alpha_2)\left[1 - \frac{tan(\alpha_2)}{tan(\phi)}\right]^{0.5} \tag{6}$$

in which $\alpha 1$ and $\alpha 2$ are the longitudinal and lateral bed slope, and ϕ the angle of natural repose (taken as 45° in this study). Because in this study, waves and currents approach from almost all angles, it is hard to distinguish longitudinal and lateral slopes. Furthermore, for the falling apron part of the scour protection, the bed slope α is close to ϕ, resulting in very low K-factors and thus high movement (see Figure 8A-C). This is in contrast to observations in the laboratory, where most of the falling apron part turned out to be stable. This led to the different formulation (Eq. 2), which showed a better comparison with laboratory observations.

Equations 5 and 6 originate from Van Rijn (1993), which were originally developed for the movement of smaller sandy material. It is assumed that these are not fully applicable to large rocks under steep slopes. Probably, effects such as embedding of the falling apron stones in the seabed and interlocking by surrounding stones are not included in this formulation. Therefore, in this study it is chosen to adopt a simple formulation that does not include the angle of repose. This is in line with common formulae for stone stability in rubble mound breakwaters, where stones are stable under steep angles. These formulae are a function of the rock slope, excluding the angle of repose (i.e., Hudson (1959); Van der Meer (1987)).

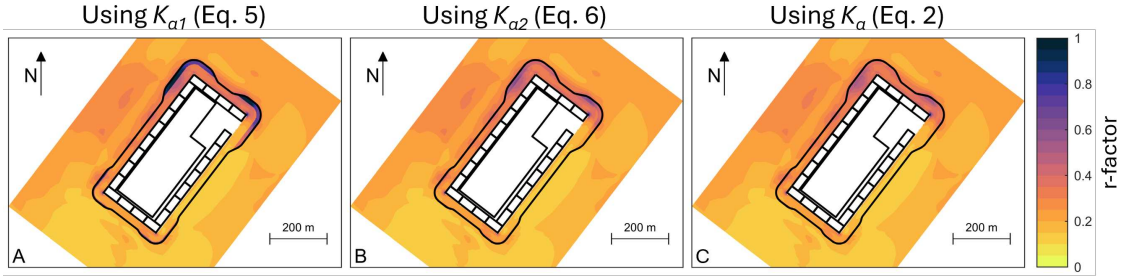

Figure 8: Movement factor r for three different ways to account for the bed slope effect.